processes

Article

Flow Characteristics Analysis of a 1 GW Hydraulic Turbine at Rated Condition and Overload Operation Condition

Chengming Liu [1], Siyuan Wu [2], Xingxing Huang [3], Shuai Zhang [2], Lingjiu Zhou [1], Tianli Hu [2] and Zhengwei Wang [4,*]

[1] College of Water Resources and Civil Engineering, China Agricultural University, Beijing 100083, China; lamous3006@163.com (C.L.); zlj@cau.edu.cn (L.Z.)
[2] Baihetan Engineering Construction Department, China Three Gorges Construction Engineering Corporation, Chengdu 610031, China; wu_siyuan@ctg.com.cn (S.W.); zhang_shuai1@ctg.com.cn (S.Z.); hu_tianli@ctg.com.cn (T.H.)
[3] S.C.I. Energy, Future Energy Research Institute, Seidengasse 17, 8706 Zurich, Switzerland; xingxing.huang@hotmail.com
[4] State Key Laboratory of Hydroscience and Engineering, Department of Energy and Power Engineering, Tsinghua University, Beijing 100084, China
* Correspondence: wzw@mail.tsinghua.edu.cn

Abstract: Flow stability is extremely important for hydraulic turbines, especially for 1 GW hydraulic turbines, and has a strong impact on mesh stability. However, turbines often operate under non-design conditions, and current research on this aspect is still lacking. So a model of the fluid domains of a high-quality installed 1 GW Francis turbine was established to investigate the flow characteristics of the turbine and fluid domains. CFD simulations of a 1 GW Francis turbine under rated load and overload operation conditions were performed. According to simulation results, when the turbine is under the overload operation condition, the internal flow stability of the 1 GW hydraulic turbine can be obviously different from that of the rated load. In the overload condition, the flow field is more turbulent and a large number of vortices are generated in the draft tube, resulting in significant changes in pressure, flow rate, and output. In order to improve calculation accuracy, a pure clearance model containing only clearances and pressure balance pipes was established. The results of the full flow channel and pure clearance were compared. It was found that under the rated operating condition and the overload condition, compared with the pure clearance model, the axial force of the runner calculated by the full flow channel model is approximately 2–7% biased, the radial force is biased by approximately 7–8%, and the leakage flow is smaller.

Keywords: 1 GW Francis turbine; pure clearance; overload condition; CFD; nonlinear fitting

Citation: Liu, C.; Wu, S.; Huang, X.; Zhang, S.; Zhou, L.; Hu, T.; Wang, Z. Flow Characteristics Analysis of a 1 GW Hydraulic Turbine at Rated Condition and Overload Operation Condition. *Processes* **2024**, *12*, 255. https://doi.org/10.3390/pr12020255

Academic Editors: Krzysztof Rogowski and Ireneusz Zbicinski

Received: 19 December 2023
Revised: 9 January 2024
Accepted: 22 January 2024
Published: 24 January 2024

1. Introduction

Hydropower is the most widely used form of clean and renewable energy, and it generates electricity by harnessing the energy of flowing and/or falling water. In the context of global climate change and the energy crisis, hydropower is increasingly playing an important role in power generation and provides numerous economic, social, and environmental benefits. With the economic development of developing countries and the continuous progress of hydroelectric generating unit technology, the demand for large and giant hydroelectric generating units, such as 1 GW units, is increasing in the power grid. Large and giant hydroelectric generating units can further ensure the safety and stability of the power grid and promote the vigorous development of clean energy.

In order to meet grid dispatchment requirements, Francis turbines have to be used under unreasonable and extreme conditions. Under these conditions, the flow state inside the Francis turbine can be very unstable. Experts have studied the pressure pulsation and hydraulic stability of giant Francis turbines at various loads both numerically and experimentally [1–4]. Pressure pulsation in the vaneless area and the draft tube is the main cause of vibration and noise in the unit. Under some operating conditions, vortex ropes and vortices are generated in the draft tube. In addition, vortices are also generated inside the runner flow channel and in the clearances, causing fluctuations in the axial force and radial force of the runner and causing vibration of the runner. Some scholars have used CFD simulations to calculate the flow pattern of the draft tube of a high-head and large Francis turbine [5,6] and researched the reason for the pressure fluctuation in the draft tube and the law of the vortex rope, which can offer better understanding of the safe and reliable operation of the turbine. Due to the large size of structures such as draft tubes, giant Francis turbines are prone to generating greater vortices and vibrations. The vortices in the draft tubes of giant Francis turbines can easily pose a huge threat and impact other flow channels and units.

Some characteristics of giant Francis turbines have been studied by some scholars. Since the flow rate of a giant Francis turbine is very large, especially at overload and full loads, the unstable flow in the turbine passage under overload conditions may cause strong vibration and potentially damage the turbine unit, threatening the safe operation of the unit [7]. Scholars reveal the dynamic excitation vibration mechanism inside the Francis turbine flow field by studying the pressure pulsation amplitude and frequency [8–10]. Numerous studies show that the noise and vibration of Francis turbines are related to pressure fluctuations [11]: mainly because the pressure changes the axial forces [12–14]. Some researchers have studied the instability and dangerous power swings at full load of a prototype Francis turbine from investigations on a reduced-scale model [15,16]. Experts have performed numerical simulations of pressure oscillations in large Francis turbines at partial and full load operating conditions and their effects on the runner structure and fatigue life. Turbines are more susceptible to cracks and damage when operating at part load [17].

For giant Francis turbines with power of 1 GW, movement of the runner has a significant impact on the internal flow characteristics at the rated condition; it especially changes the radial force and axial force [18–23]. Gong [24] conducted a numerical simulation of pressure fluctuation in a 1000 MW Francis turbine under a small opening condition and found that unstable flow leads to increased instability. Liu et al. [25] investigated the effects of head and flow rate on the pressure and velocity characteristics of a 1 GW Francis turbine and found that there is a significant difference in the pressure and velocity fields under different operating conditions. Chen [26] studied the internal flow characteristics of long and short blade runners of a 1000 MW Francis turbine under different opening conditions and concluded that an increase in volume led to an increase in dynamic and static interference. However, up to now, there has been very limited research focused on the internal flow characteristics under overload conditions of giant Francis turbines.

In order to analyze the reasons why giant Francis turbines produce vibrations and noise under overload conditions, a 3D model of the flow channel of a 1 GW Francis turbine unit was built in this study. Next, the finite element mesh of the flow channels of the 1 GW Francis turbine was established to analyze the internal flow characteristics. Sensitivity analysis of the flow domain mesh was conducted and was calibrated with measurement results. Then, the internal flow characteristics of a 1 GW Francis turbine unit under rated load and overload operation conditions were calculated by means of CFD simulations. In order to improve the calculation accuracy of the overload condition and the rated condition, a pure clearance model containing only clearances and pressure balance pipes was established. The results, such as the axial force, radial force, and leakage flow under the rated condition and the overload condition, were compared and discussed in detail.

2. Numerical Calculation Methods

The Reynolds numbers of the flow in giant Francis turbine units are high, and the flow is more violent and the flow pattern is more variable. Direct methods are generally not used to solve the NS equations. Therefore, the Reynolds time-averaged method is used in this paper. The Reynolds average method is a indirect numerical simulation method to decompose the turbulent velocity and pressure into an average and a pulsation. We are only concerned about the conversion of mechanical energy in this paper, so the internal flow control equations of giant turbines only have mass conservation equations and momentum conservation equations. For the fluid of a Francis turbine, the internal flow is incompressible. The flow domain is calculated by the RANS equations:

$$\frac{\partial}{\partial x_i}(\overline{u_i}) = 0 \tag{1}$$

$$\frac{\partial}{\partial t}(\overline{u_i}) + \frac{\partial}{\partial x_j}(\overline{u_i u_j}) = -\frac{1}{\rho}\frac{\partial \overline{p}}{\partial x_i} + \frac{\partial}{\partial x_j}\left[\nu\left(\frac{\partial u_i}{\partial x_j} + \frac{\partial u_j}{\partial x_i}\right)\right] - \frac{\partial \overline{u_i' u_j'}}{\partial x_i} + f_i \tag{2}$$

where u_i, u_j are directional components of velocities, and x_i, x_j are coordinates in the rectangular coordinate system; ρ and p are the density and pressure of fluid, respectively; t is time, v is kinematic viscosity, and f_i is volume force.

A shear stress transport (SST) model considers the transmission of turbulent shear stress. The k-ω model is used in the near wall area and the k-$\mathcal{E}$ model is used in the turbulent core area. The results of near-wall flow calculated by the SST model are more accurate. And the model also has high reliability in the calculation of the reverse pressure gradient. The internal flow field of a giant Francis turbine is mainly turbulent flow. Therefore, in order to ensure that the simulation results are closer to reality, the SST model is used for calculations in this article.

3. Calculation Model of a 1 GW Francis Turbine Unit

The fluid domain model of the investigated 1 GW Francis turbine is shown in Figure 1. The model consists of the flow passages of the spiral case, stay vane, guide vane, runner, upper crown, lower ring, labyrinth seals, draft tube, and pressure balance pipes [25]. The parameters of the 1 GW Francis turbine studied in this paper are shown in Table 1. The parameters for the rated condition and overload condition are shown in Table 2.

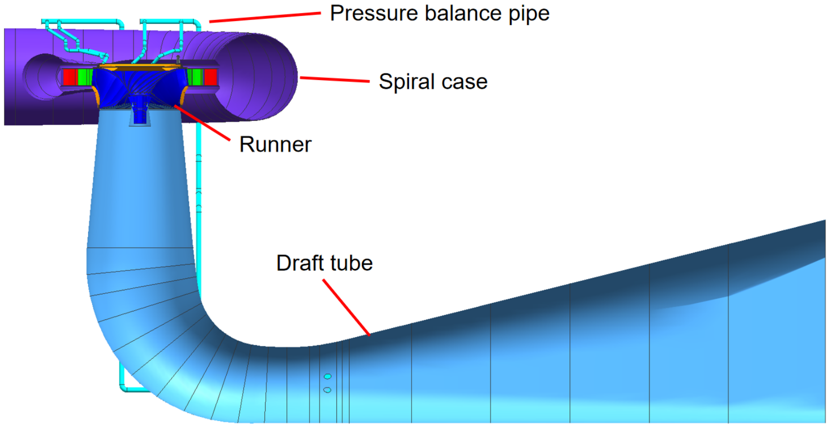

Figure 1. Flow domain model of the 1 GW Francis turbine unit.

Table 1. Parameters of giant Francis turbine.

Parameter	Value
Rated power	1000 MW
Rated speed	111.1 rpm
Rated head	202 m
Number of stay vanes	23
Number of guide vanes	24
Number of runner blades	15

Table 2. Parameters under the rated condition and overload condition.

	Guide Vane Opening (°)	Head (m)	Output (MW)	Head at the Outlet of the Draft Tube (m)
Rated condition	27.8	202	1015	49.02
Overload condition	28.2	213	1100	22

4. Mesh Sensitivity Analysis of the 1 GW Francis Turbine Unit

A structured hexahedral mesh and an unstructured tetrahedral mesh are important for improving the computational accuracy and efficiency. In order to improve the computational accuracy, the turbine model in this paper combines the two for the flow field of a giant Francis turbine. Since the spiral case and discharge cone contain a large number of irregular structures, a well-adapted unstructured mesh is used for this part of the mesh. The guide vane, stay vane, runner, draft tube, upper crown and lower ring clearance, and pressure balance pipe have more regular structures and are divided by a hexahedral structured mesh that saves more storage space and computes faster. In this article, ICEM and mesh software are used to create the mesh. The software ANSYS-CFX 19.1 is selected for simulation. The overall mesh quality is great, and the mesh model is shown in Figure 2 following.

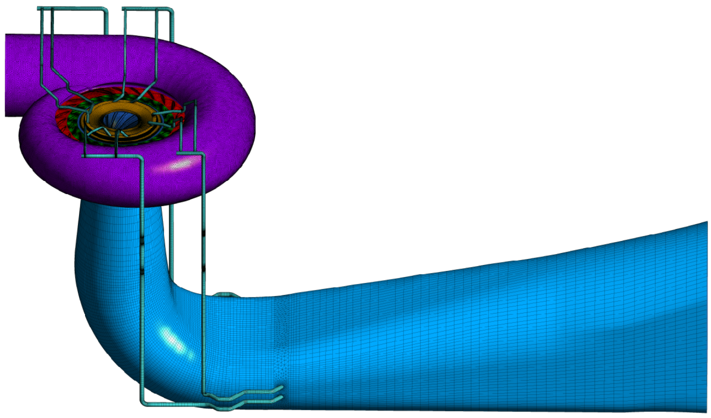

Figure 2. Mesh of the flow domains of the 1 GW Francis turbine unit.

The quantity and quality of the mesh have a significant impact on the calculation results. In order to minimize the impact of the mesh, the grid convergence index (GCI) is used to verify the reliability of the mesh [27–29]. The basic idea is to establish a relationship based on the proportional relationship between the approximation error and the true error. The approximate and extrapolated relative errors can be expressed as:

$$\varepsilon_a = 100\% \times \left| \frac{\varepsilon_{new} - \varepsilon_{old}}{\varepsilon_{new}} \right| \tag{3}$$

The grid convergence index (GCI) can be written as:

$$GCI = \frac{1.25 \times \varepsilon_a}{r^2 - 1} \tag{4}$$

where ε_a is the relative error, and r is the mesh ratio, which is 1.3. A total of three sets of different numbers of meshes (2.4×10^6, 5.0×10^6, 1.02×10^7) are set up, and the mesh quality of the giant Francis turbine under the rated condition is compared with the change to the number of meshes (refer to Table 3). As is shown, the set of 10.2 million meshes shows lower uncertainty. Therefore, the final number of elements is 10.2 million. Table 4 shows the number of meshes for each channel.

Table 3. The mesh quality of the giant Francis turbine.

	Normalized Efficiency	ε_a (%)	*GCI*
2.4×10^6	0.979	0.7	1.268
5.0×10^6	0.986	0.5	0.905
1.02×10^7	0.991	0.1	0.181

Table 4. The number of elements for the flow passages of the 1 GW Francis turbine unit.

Flow Passage	Element Number	Element Type
Runner	2.60×10^6	Tetrahedral and hexahedral
Band chamber	2.47×10^6	Hexahedral
Spiral case	1.55×10^6	Tetrahedral
Pressure balance pipes	1.04×10^6	Hexahedral
Draft tube	0.93×10^6	Tetrahedral and hexahedral
Crown chamber	0.78×10^6	Tetrahedral and hexahedral
Guide vane	0.76×10^6	Hexahedral
Stay vane	0.38×10^6	Hexahedral
Total	10.51×10^6	Tetrahedral and hexahedral

There must be some differences between the simulated and modeled results due to various factors such as model accuracy and the size of the clearance flow. Therefore, it is necessary to verify the accuracy of the model before the simulations. In order to verify that the differences between the simulated and experimental results are within reasonable limits, the simulated and experimental values of the efficiencies at four head conditions are compared. The experimental values were measured on-site through a prototype giant Francis turbine at a hydropower station. The results are shown in Figure 3. Therefore, the simulation results in this paper have small differences compared to the experimental results and thus can reflect real turbine operation results and provide important reference values for the actual project.

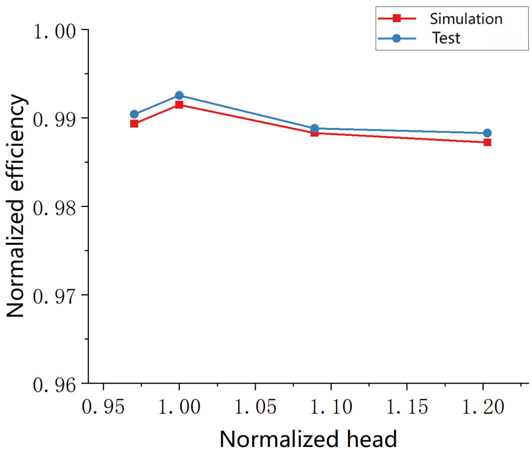

Figure 3. Comparison between simulation and test efficiency.

5. Mesh and Computational Settings of the Pure Clearance Domain

In order to improve the accuracy of axial and radial forces, the meshes of the upper clearance, the lower ring clearance, and the pressure balance pipes will be retained in this section. All the remaining fluid domains are removed, and the number of meshes of the upper crown clearance and lower ring clearance are increased. Then, calculations for the rated and overload conditions are performed. The model of the computational domain is shown in Figure 4. The boundary conditions of the inlet of the upper crown and the lower ring are set to the velocity inlet, the outlet is set to the pressure outlet, and the conditions of the inlet and outlet are set to the calculation results of the full flow channel.

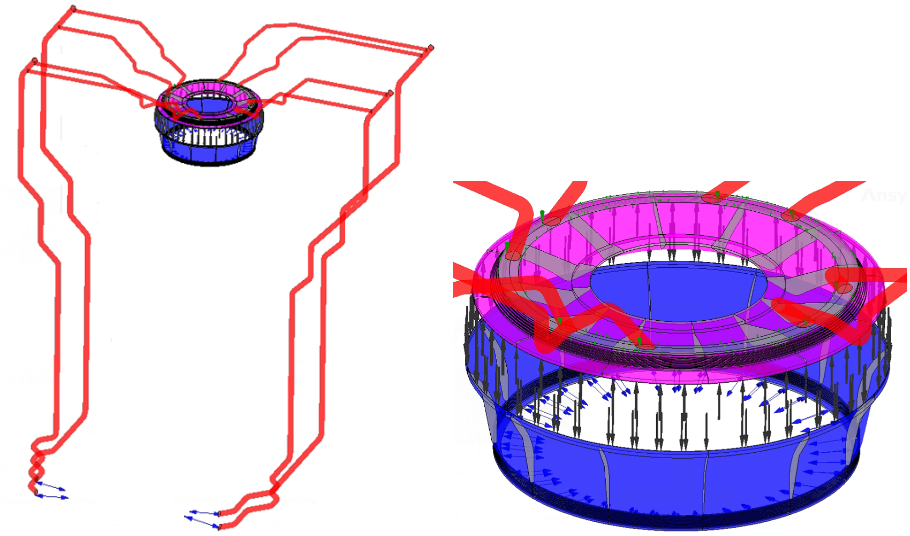

(**a**) Overall (**b**) Inlet of the pure clearance

Figure 4. The computational domain of the pure clearance.

In order to ensure the accuracy of the calculation of the clearance, the axial and radial forces on the outer surface of the upper crown and on the outer surface of the lower ring under rated working conditions are used as a reference. Under the condition of ensuring that the pressure difference between the inlet and outlet of the clearance is consistent, the irrelevance of the mesh is verified. For calculations of the pure clearance, focus is placed on the reliability of its axial and radial force predictions. Therefore, the sensitivity of the axial and radial forces to the mesh was mainly investigated, and a total of seven sets of meshes were established. The calculation results are shown in Table 5. It can be seen that when the number of meshes is 10 million, the axial force on the outer surface of the upper crown is basically stable, and when the number of meshes is 12 million, the axial and radial forces on the outer surface of the lower ring are basically stable. On the basis of reducing the amount of calculation, a set of 12 million meshes is used for subsequent solution analysis.

Table 5. Verification of mesh independence of the pure clearance domain.

Number of Meshes (Million)	Axial Force on Outer Surface of Lower Ring (kN)	Axial Force on Outer Surface of Upper Crown (kN)	Radial Force on Outer Surface of Lower Ring (kN)	Radial Force on Outer Surface of Upper Crown (kN)
4	22,200	30,550	2.76	6.77
6	22,630	30,700	2.80	6.81
8	22,870	30,910	2.83	6.84
9	23,000	31,090	2.85	6.86
10	23,380	31,250	2.87	6.89
12	23,460	31,280	2.91	6.92
23	23,470	31,290	2.92	6.93

6. Results and Discussions

6.1. Pressure Distributions

The pressure distribution of the axial cross-section and the central cross-section of the full flow channel are shown in Figures 5 and 6. Normalized pressure is the pressure divided by the maximum pressure value in the flow channel. The pressure distribution is similar for both conditions, with a gradual decrease in the pressure from inlet to outlet. Pressure is lower in the upper crown clearance and in the flow channel of the runner cone.

Although the head under the overload condition is larger than that of the rated condition, the pressure in the flow channel under the overload condition is overall smaller than that of the rated condition because the head at the outlet under the overload condition is smaller. It can be seen through Figure 6 that along the runner channel, the pressure of the fluid gradually decreases and the pressure on the pressure surface is greater than that on the suction surface. The pressure in the runner cross-section reaches a minimum at the outlet of the suction surface. Unlike in the rated condition, there is a pressure increase in the elbow section of the draft tube in the overload condition due to vortices.

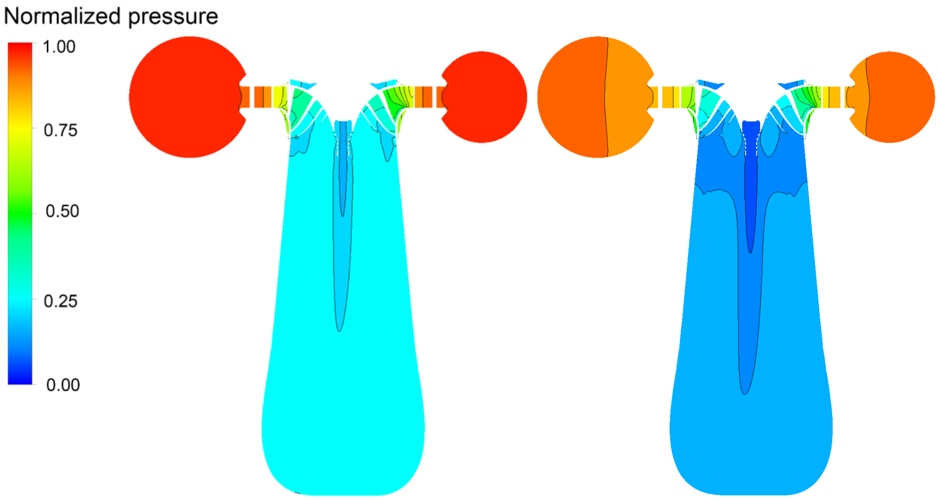

(**a**) Rated condition (**b**) Overload condition

Figure 5. The pressure distribution of the vertical cross-section of the full flow channel.

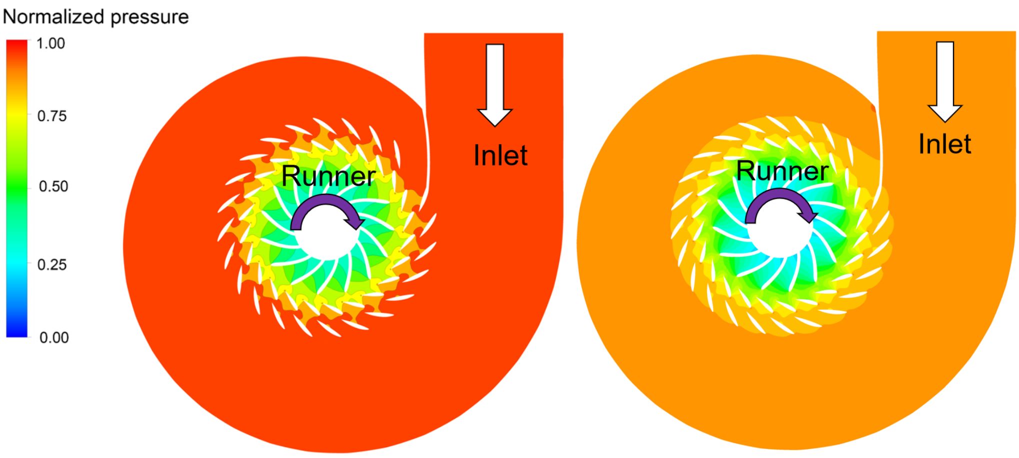

(**a**) Rated condition (**b**) Overload condition

Figure 6. The pressure distribution of the horizontal cross-section of the full flow channel.

6.2. Streamlines and the Pressure Distribution in the Runner Channel

Figures 7 and 8 show the pressure and streamline distributions of the runner channel, respectively. Normalized velocity is the velocity divided by the maximum velocity value in the flow channel. The pressure distribution on the surface of the runner is similar in both conditions. The pressure distribution on the surface of each blade is the same. From the inlet of the runner to the outlet of the runner, the pressure on the surface of the runner decreases uniformly, and the velocity of the fluid in the runner channel increases gradually. Because the fluid coming out of the vaneless zone impinges on the surface of the blades as it flows into the runner channel, the pressure is highest at the inlet of the runner blades, and the streamlines change along the shape of the blades. Inside the runner channel, the flow rate is highest, and the pressure is lowest at the outlet of the runner. Since the overall pressure on the turbine is greater under the rated condition than that under the overload condition, the pressure on the runner channel under the rated condition is also slightly greater than that under the overload condition.

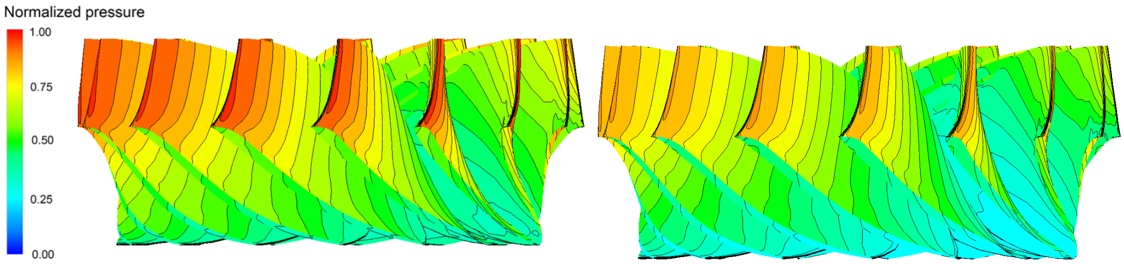

(**a**) Rated condition (**b**) Overload condition

Figure 7. The pressure distribution of the runner channel.

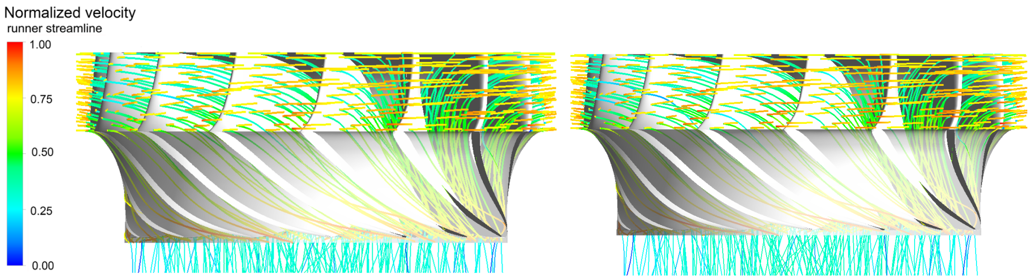

(**a**) Rated condition (**b**) Overload condition

Figure 8. The streamlines of the runner channel.

6.3. Streamline Distribution

Figure 9 shows the densities and shapes of streamlines of the full channel flow under the rated and overload conditions. For the rated condition, vortices are almost not present in the full flow channel of the turbine. The flow in the flow channel is essentially stable and meets the setup goals for the rated conditions. In the overload operating condition, the flow pattern in the draft tube is more turbulent. Figure 10 shows a cross-sectional view of streamlines in the draft tube. It can be seen that there are vortices in the elbow section of the draft tube, and the vortices gradually increase and move towards the outlet direction. The streamlines are mainly concentrated on the lower side wall surface of the draft tube.

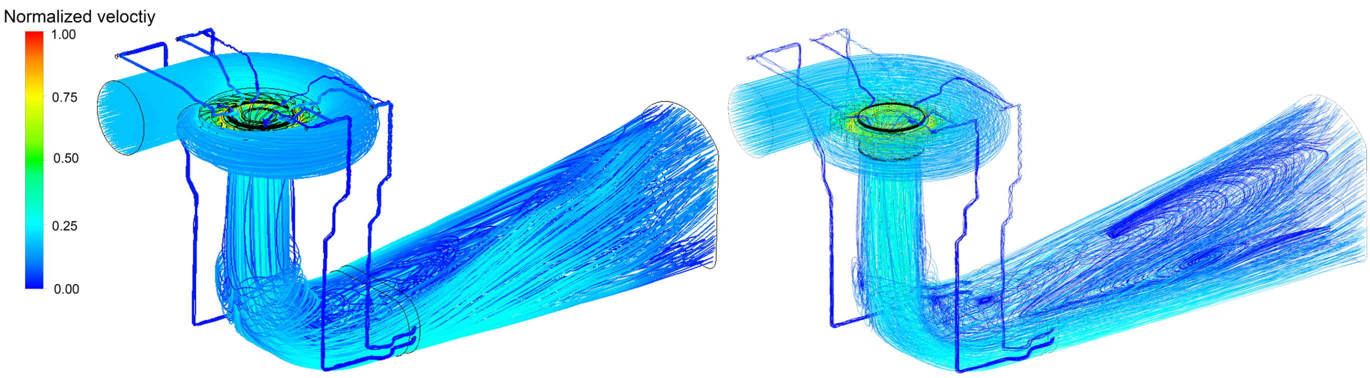

(**a**) Rated condition (**b**) Overload condition

Figure 9. The streamline distribution of the full flow channel.

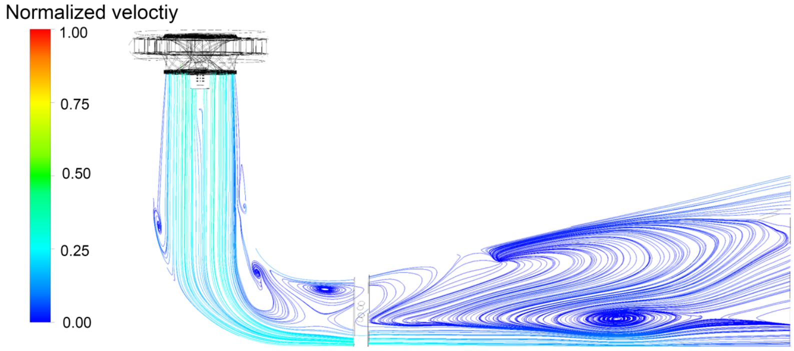

Figure 10. The streamline contours in the draft tube under the overload operating condition.

6.4. Pressure Fluctuate

In order to study the pressure characteristics in the draft tube, several pressure monitoring points were arranged in the draft tube; the locations of the monitoring points (W1, W2, W3, W4, W5) are shown in Figure 11. Moreover, Figure 12 shows the pressure monitoring results under the overload operating condition, and it can be seen that from the inlet of the draft tube to the outlet, the pressure in the flow channel decreases gradually. Only the pressures of W3 and W4 are similar. The pressure values at all monitoring points fluctuate greatly with time, with a fluctuation range of about 10 kPa. The pressure fluctuations in the draft tube were mainly influenced by the vortices in the flow. It is these pressure fluctuations that lead to large vibrations in the unit under overload operating conditions, which seriously threatens the safety of the unit structure.

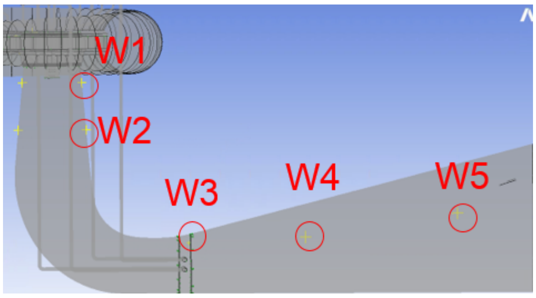

Figure 11. The monitoring points in the draft tube.

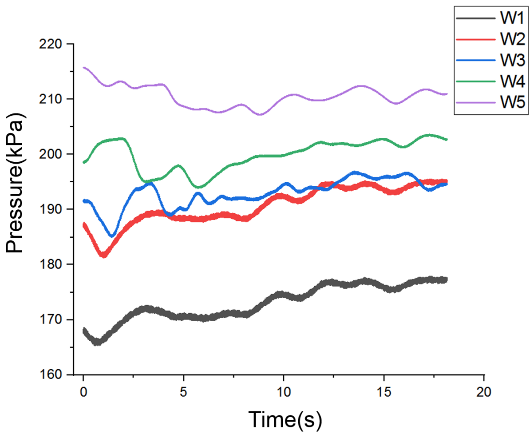

Figure 12. The pressure fluctuations in the draft tube.

6.5. Hydraulic Characteristics under the Overload Condition

Figure 13 shows the flow rate and output of the unit under the overload operating condition. It can be seen that the curves of the flow rate and output are similar in that they both fluctuate considerably with time, and there is no periodic pattern. The flow rate stays between 590–592 m^3/s. The output power fluctuates between 1095–1105 MW with a large difference. This indicates that the vortices under the overpower condition cause a large amount of energy waste and reduce the power generation, which is not conducive to the long-term efficient and stable operation of the unit.

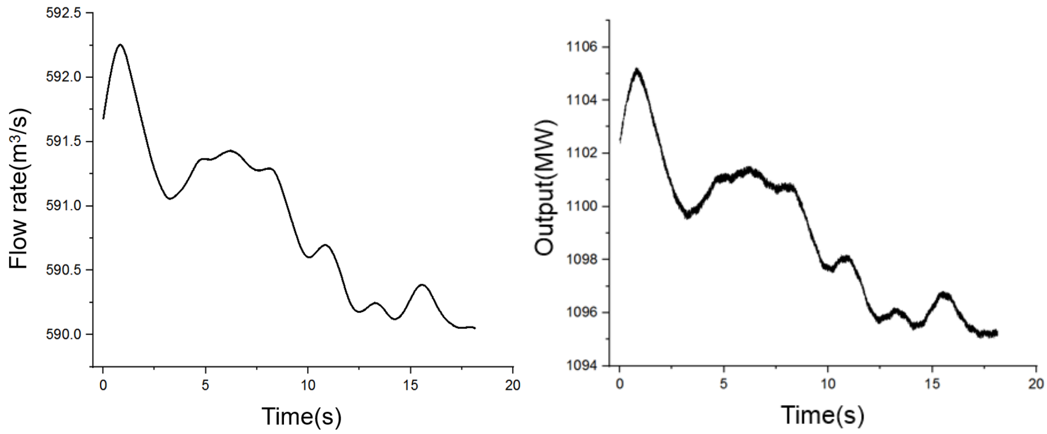

(**a**) Flow rate (**b**) Output

Figure 13. The flow rate and output under the overload condition change over time.

7. Calculation Results of the Pure Clearance Domain

7.1. The Leakage Flow and the Axial Speed in the Labyrinth Ring

By changing the inlet velocity of the pure clearance, the pressure difference between the inlet and outlet of the clearance is obtained as the leakage flow changes. The clearance inlet and outlet pressure difference and the leakage flow are fitted into a curve. The inlet velocity of the pure clearance is selected by ensuring that the pressure difference between the inlet and outlet of the pure clearance model is the same as that of the full flow channel model. Figure 14 shows the relationship curve under the rated condition. It can be seen that the relationship between the leakage flow and the pressure difference is close to a linear relationship. The inlet velocity of the pure clearance model is also obtained by the same method for the overload condition.

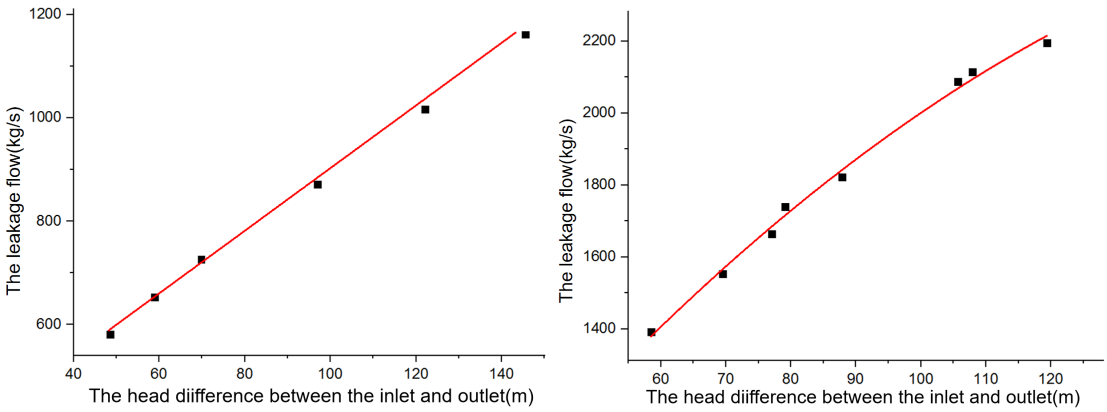

(**a**) The upper crown (**b**) The lower ring

Figure 14. The leakage flow of pure clearance changes with the pressure difference between the inlet and outlet.

Table 6 shows the leakage flow of the full flow channel and pure clearance under the rated condition and the overload condition. The results show that under the rated condition, when the inlet and outlet pressure differences of the clearances between the two models are the same, the leakage flow of the full flow channel is larger than that of the pure clearance. The same result is found in the overload condition.

Table 6. Calculation results of leakage flow of the full flow channel and pure clearance.

	Leakage Flow of the Lower Ring of Full Flow Channel (kg/s)	Leakage Flow of the Upper Crown of Full Flow Channel (kg/s)	Leakage Flow of the Lower Ring of Pure Clearance (kg/s)	Leakage Flow of the Upper Crown of Pure Clearance (kg/s)
Rated condition	1771	916	2180	987
Overload condition	1675	731	1865	760

In order to analyze the reasons for the change in leakage flow, the axial velocities on the cross-sectional diagrams of the full flow channel and the pure clearance under the rated condition are shown in Figures 15 and 16, respectively. The axial velocity distribution rules in the labyrinth rings of the two sets of meshes are different. The number of labyrinth ring meshes in the full flow channel is small and the axial velocity is small, while the axial velocity of the fluid at the labyrinth ring in the pure clearance is larger. Therefore, the flow rate difference between the two sets of meshes in the labyrinth ring is large, and the leakage flow is also quite different.

The formulas for the pressure coefficient C_p and speed coefficient C_v are:

$$C_p = \frac{P}{\rho g H_r} \tag{5}$$

$$C_v = \frac{v}{\frac{2\pi n R}{60}} \tag{6}$$

where P is the pressure value measured at the measuring point, Pa. H_r is the rated head of 202 m for the turbine, v is the measuring-point speed, m/s, n is the rotation speed of the runner, which is 111.1 r/min, and R is the entrance radius of the runner, which is 4.235 m.

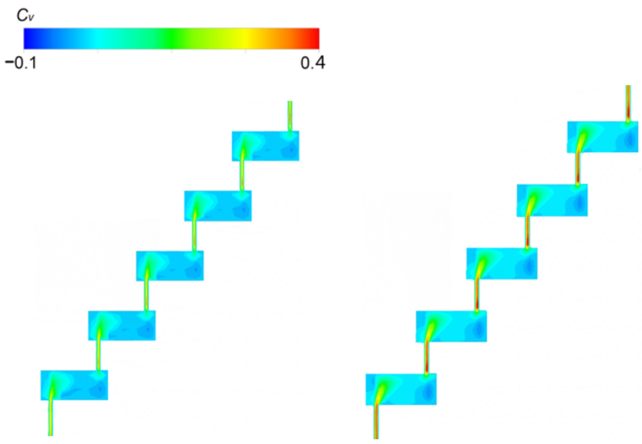

(**a**) Full flow channel (**b**) Pure clearance

Figure 15. The C_v of the axial velocity in the labyrinth ring of the upper crown clearance.

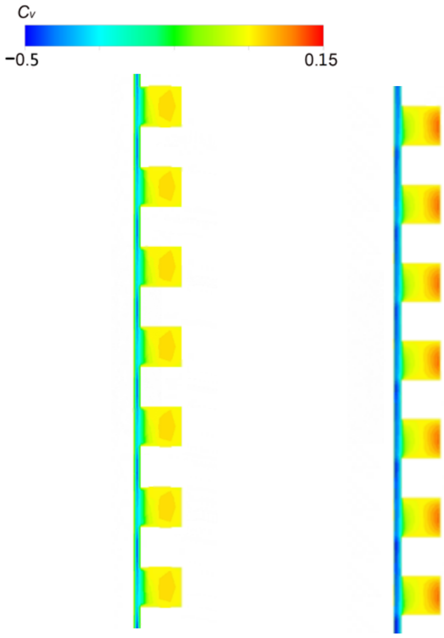

(a) Full flow channel (b) Pure clearance

Figure 16. The C_v of the axial velocity in the labyrinth ring of the lower ring clearance.

7.2. The Force and Pressure of the Clearance

The pure clearance was used to calculate the axial force on the outer surface of the upper crown, the lower ring of the runner and the radial force of the runner in the two working conditions, as shown in Table 7. In the calculation of the axial force and radial force of the runner, the calculation results of the full flow channel are used for the forces on other surfaces. It can be seen that the axial force and the radial force of the runner under the rated working condition are larger than those under the overload condition. Moreover, the prediction of the radial force and axial force by the full flow channel model is larger.

Table 7. Force calculation results for full flow channels and pure clearance meshes.

	Runner Radial Force of Pure Clearance (kN)	Runner Axial Force of Pure Clearance (kN)	Runner Radial Force of Full Flow Channel (kN)	Runner Axial Force of Full Flow Channel (kN)
Rated condition	60	9650	65	10,300
Overload condition	56	7829	60	8034

The axial force and radial force of the unit mainly depend on the pressure changes in the upper crown clearance and lower ring clearance. The greater the pressure in the clearance, the greater the force of water on the unit. The smaller the pressure in the clearance, the smaller the force of water on the unit. Figure 17 shows the ZX cross-section pressure distribution in the runner and clearance channel under the rated condition and the overload condition. When the fluid enters the clearance, the pressure does not change much. After the fluid enters the labyrinth ring, the pressure drops significantly due to the extremely small size of the labyrinth ring. The area of the clearance domain behind the labyrinth ring gradually increases, and a large number of low-pressure areas are generated at the upper crown cavity and the outlet of the lower ring, resulting in an unstable flow state.

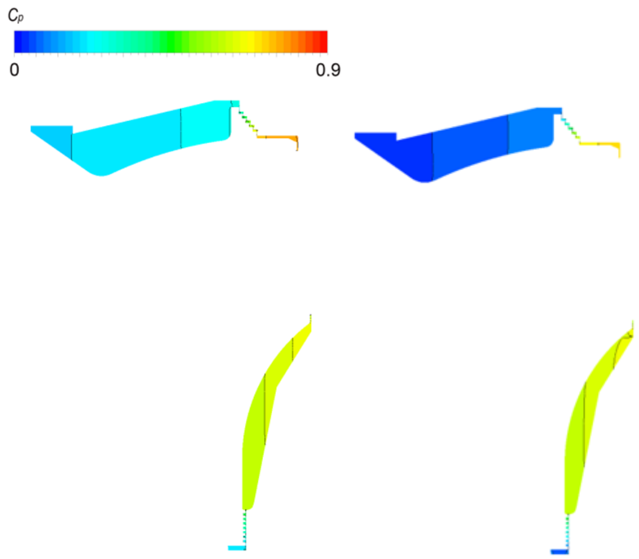

(**a**) Rated condition (**b**) Overload condition

Figure 17. Pressure in the clearance.

Figure 18 shows the location of the lines for monitoring pressure and the results of monitoring the pressure in the lower ring. Figure 19 shows the location of lines for monitoring pressure and the results of monitoring the pressure in the upper crown. It can be seen that the pressure changes in the clearance between the upper crown and the lower ring can be divided into three areas: the cavity outside the seal, the sealing area, and the cavity inside the seal.

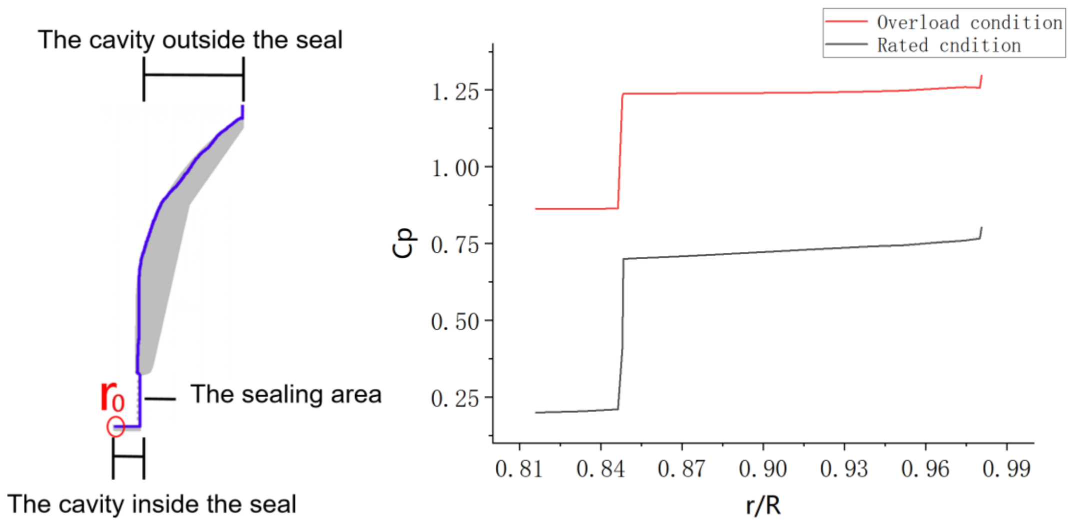

(**a**) Lines for monitoring pressure (**b**) Results of monitoring the pressure

Figure 18. Results of monitoring the pressure in the lower ring clearance.

It is generally believed that due to the rotation of the runner, the water pressure in the sealing area can be approximately linearly distributed. The pressures in the cavity outside the seal and the cavity inside the seal show quadratic curves as the radius increases, and their analytical expressions can be written as:

$$p = p_0 + \frac{1}{2}\rho\omega^2(r^2 - r_0^2) = p_0 + \frac{1}{2}\rho\left(\frac{K_0\pi n}{30}\right)^2(r^2 - r_0^2) \tag{7}$$

$$K_0 = \frac{\omega}{\omega_0} \tag{8}$$

where r_0 and p_0 are the radius and static pressure, respectively, at a known point: the positions are shown in Figures 18 and 19. K_0 is the ratio of the average circumferential angular velocity in the clearance to the rotational angular velocity of the runner. It is generally considered to be about 0.5 without considering the secondary flow in the gap. However, there are also complex vortex structures in the actual flow pattern in the cavity that affect the pressure distribution in the cavity. Therefore, quadratic nonlinear fitting and linear fitting are performed on each curve under non-operating conditions.

The function for the pressure of the cavity outside the seal of the lower ring under the rated condition after quadratic fitting is

$$p = 1{,}377{,}840 + 25{,}455(r^2 - 3.73^2) \quad (9)$$

The function for the pressure of the cavity inside the seal of the lower ring under the rated condition after quadratic fitting is

$$p = 391{,}676 + 20{,}862(r^2 - 3.59^2) \quad (10)$$

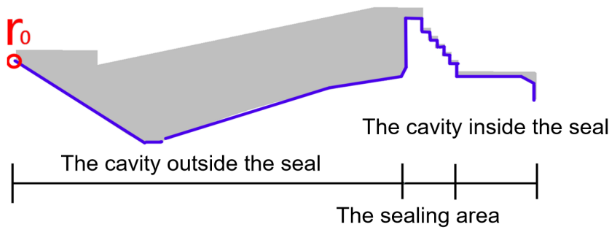

(**a**) Lines for monitoring pressure

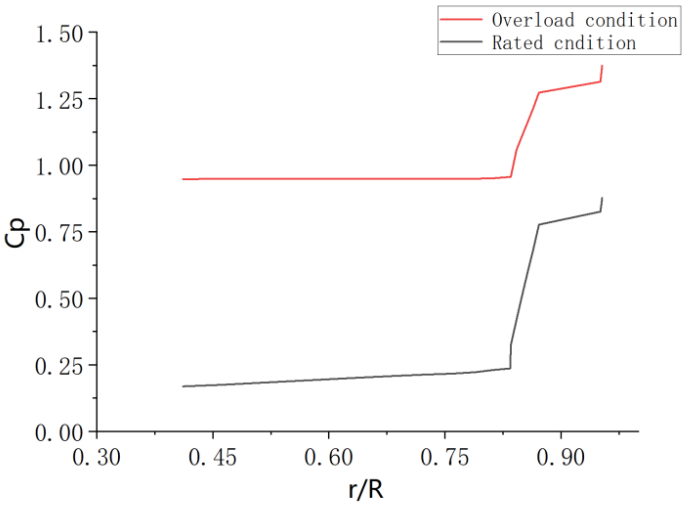

(**b**) Results of monitoring the pressure

Figure 19. Results of monitoring the pressure in the upper crown clearance.

The function for the pressure of the cavity outside the seal of the upper crown under the rated condition after quadratic fitting is

$$p = 1{,}535{,}970 + 18{,}389(r^2 - 3.87^2) \quad (11)$$

The function for the pressure of the cavity inside the seal of the upper crown under the rated condition after quadratic fitting is

$$p = 332{,}662 + 12{,}709(r^2 - 1.81^2) \quad (12)$$

The function for the pressure of the cavity outside the seal of the lower ring under the overload condition after quadratic fitting is

$$p = 839{,}869 + 9683(r^2 - 3.73^2) \quad (13)$$

The function for the pressure of the cavity inside the seal of the lower ring under the overload condition after quadratic fitting is

$$p = 103{,}626 + 4205(r^2 - 3.59^2) \quad (14)$$

The function for the pressure of the cavity outside the seal of the upper crown under the overload condition after quadratic fitting is

$$p = 840{,}145 + 28{,}786(r^2 - 3.87^2) \tag{15}$$

The function for the pressure of the cavity inside the seal of the upper crown under the overload condition after quadratic fitting is

$$p = 191{,}931 + 1572(r^2 - 1.81^2) \tag{16}$$

Figures 20–23 show the pressure linear fitting and quadratic fitting curves of the cavity inside the seal and the cavity outside the seal under the rated condition and the overload condition. The results show that the quadratic curve and linear curve of the cavity inside the seal are different under the rated condition, and the quadratic curves and linear curves of the pressures in the remaining cavities are almost coincident. Except for the cavity outside the seal by the upper ring, the quadratic curves and linear curves of the remaining cavities under the overload condition are somewhat different. This shows that the pressures in the cavities under the overload condition are more suitable for fitting using quadratic curves.

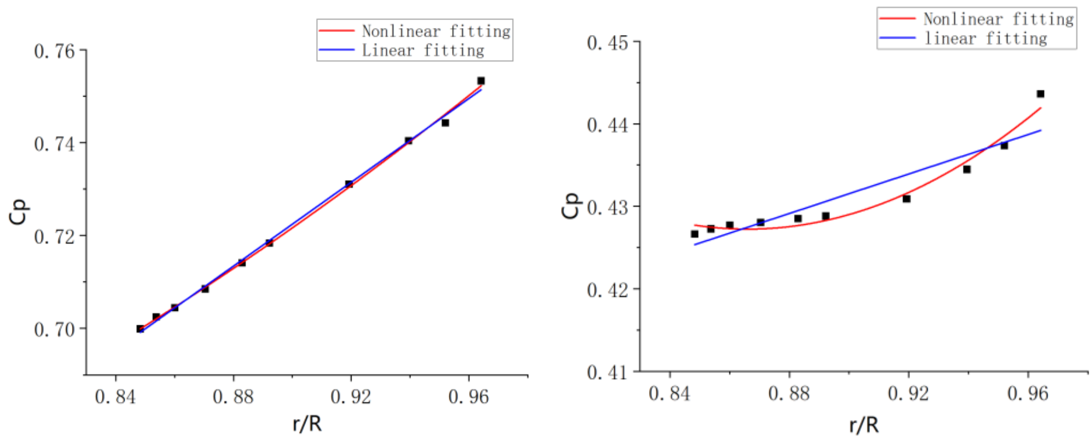

(**a**) Rated condition (**b**) Overload condition

Figure 20. Fitting curves for pressure in the cavity outside the seal of the lower ring.

The values of K_0 under the rated condition and overload condition are shown in Table 8. There is a big difference in K_0 at four positions between the rated condition and the overload condition. Only the difference in K_0 for the cavity outside the seal of the upper crown under the two working conditions is small: about 0.2. The K_0 differences for the cavity inside the seal of the upper crown, the cavity outside the seal of the lower ring, and the cavity outside the seal of the lower ring in the two working conditions are all large.

Table 8. The values of K_0 under the rated condition and overload condition.

	K_0 of the Cavity Outside the Seal in the Upper Crown	K_0 of the Cavity Inside the Seal in the Upper Crown	K_0 of the Cavity Outside the Seal in the Lower Ring	K_0 of the Cavity Inside the Seal in the Lower Ring
Rated condition	0.85	0.707	1	0.906
Overload condition	0.65	0.15	0.378	0.25

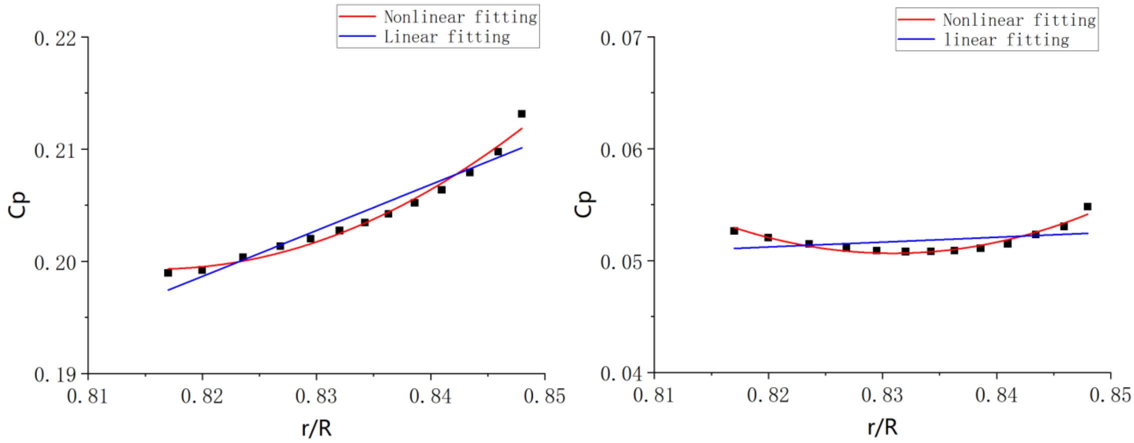

(**a**) Rated condition (**b**) Overload condition

Figure 21. Fitting curves for pressure in the cavity inside the seal of the lower ring.

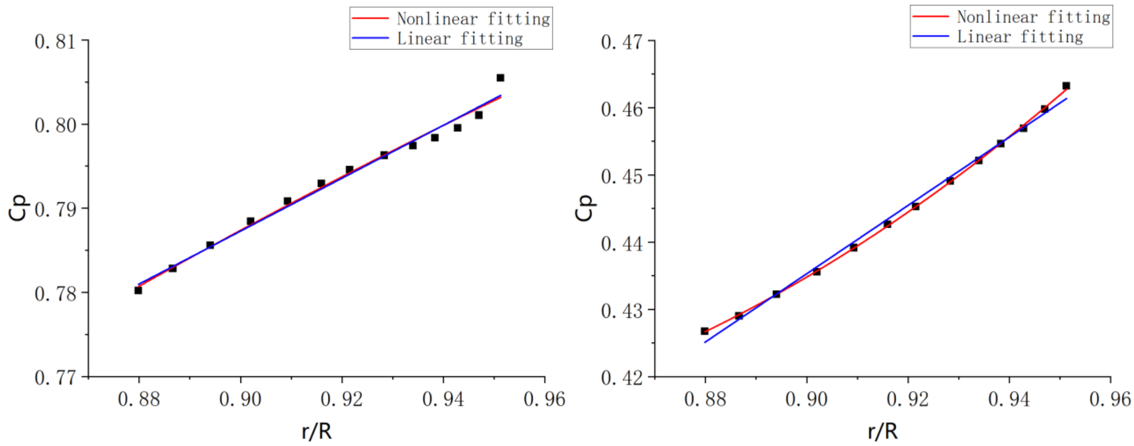

(**a**) Rated condition (**b**) Overload condition

Figure 22. Fitting curves for pressure in the cavity outside the seal of the upper crown.

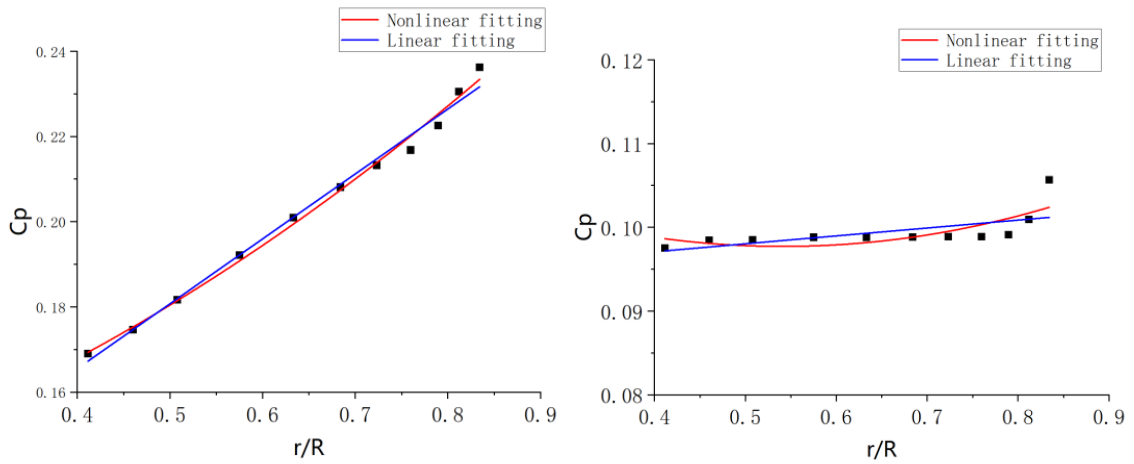

(**a**) Rated condition (**b**) Overload condition

Figure 23. Fitting curves for pressure in the cavity inside the seal of the upper crown.

8. Conclusions

In this research, the internal flow field characteristics of a 1 GW Francis turbine are analyzed under two conditions: the rated condition and overload operation. The pressure values at all monitoring points under the overload condition fluctuate greatly with time. Vortices in the flow in the draft tube under the overload condition cause fluctuations in the flow and output of the unit, and a large amount of energy is wasted, which reduces power generation and is not conducive to the efficient and stable operation of the unit over the long term.

The pure clearance is used to calculate the force and pressure characteristics under different working conditions, which improves the calculation accuracy. When the pressure difference between the inlet and outlet of the clearance is the same, the number of clearance meshes has a greater impact on the axial velocity at the labyrinth ring and changes the flow rate in the clearance. Under the same pressure difference between the inlet and outlet, compared with the full flow channel, the leakage flow of the pure clearance is larger, and the axial force and radial force are smaller.

The pressure changes in the clearance cavity of the upper crown and the lower ring can be divided into the cavity outside the seal, the sealing area, and the cavity inside the seal. Due to the rotation of the runner, the pressures in the cavity outside the seal and the cavity inside the seal show a quadratic curve as the radius increases. The pressure in the clearance is fitted to provide a reference for the subsequent calculation of the pressure and force characteristics of the giant Francis turbine.

Author Contributions: Conceptualization, Z.W. and X.H.; methodology, C.L. and X.H.; investigation, C.L., S.W., and X.H.; validation, S.Z. and T.H.; writing—original draft preparation, C.L. and X.H.; writing—review and editing, C.L., S.W. and X.H.; supervision, L.Z. and Z.W. All authors have read and agreed to the published version of the manuscript.

Funding: This work is supported by the National Natural Science Foundation of China (No. 51876099).

Data Availability Statement: Data are contained within the article.

Acknowledgments: The authors would like to thank the research project: "Multi-field coupling study on dynamic characteristics of 1000 MW hydrogenerator unit" supported by the China Three Gorges Construction Group Co., Ltd. (contract No. JGJD0322003).

Conflicts of Interest: Authors Siyuan Wu, Shuai Zhang and Tianli Hu were employed by the company China Three Gorges Construction Engineering Corporation. The remaining authors declare that the research was conducted in the absence of any commercial or financial relationships that could be construed as a potential conflict of interest.

Abbreviations

The following abbreviations are used in this manuscript:

C_p	Pressure coefficient
C_v	Speed coefficient
CFD	Computational fluid dynamics
f	Force, N
H	Head, m
n	Rotation speed
p	Pressure, Pa
r	Radius, m
RANS	Reynolds-averaged Navier–Stokes
SST	Shear stress transport
t	Time, s
u	Velocity of fluid, m/s
x	Component of position vector, m

References

1. Shi, Q. Hydraulic design of Three Gorges right bank powerhouse turbine for improvement of hydraulic stability. *IOP Conf. Ser. Earth Environ. Sci.* **2010**, *12*, 012006. [CrossRef]
2. Wang, F.J.; Liao, C.L.; Tang, X.L. Numerical simulation of pressure fluctuations in a large Francis turbine runner. *Chin. J. Mech. Eng.* **2012**, *25*, 1198–1204. [CrossRef]
3. Wang, Y.L.; Li, G.Y.; Shi, Q.H.; Wang, Z.N. Hydraulic design development of Xiluodu Francis turbine. *IOP Conf. Ser. Earth Environ. Sci.* **2012**, *15*, 032006. [CrossRef]
4. Wang, F.J.; Zhao, W.; Yang, M.; Xiao, R.F. Analysis on unsteady fluid-structure interaction for a large scale hydraulic turbine: Modeling and flow simulation. *J. Hydraul. Eng.* **2011**, *42*, 1385–1391.
5. Shi, Q. Experimental Investigation of Frequency Characteristics of Draft Tube Pressure Pulsations for Francis Turbines. In Proceedings of the Hydraulic Machinery and Cavitation, Valencia, Spain, 16–19 September 1996; Cabrera, E., Espert, V., Martínez, F., Eds.; Springer: Dordrecht, The Netherlands, 1996; pp. 935–944.
6. Ciocan, G.D.; Iliescu, M.S.; Vu, T.C.; Nennemann, B.; Avellan, F. Experimental Study and Numerical Simulation of the FLINDT Draft Tube Rotating Vortex. *J. Fluids Eng.* **2006**, *129*, 146–158. [CrossRef]
7. Kuznetsov, N.; Yuldashev, M.; Yuldashev, R. Analytical-numerical analysis of closed-form dynamic model of Sayano-Shushenskaya hydropower plant: Stability, oscillations, and accident. *Commun. Nonlinear Sci. Numer. Simul.* **2021**, *93*, 105530. [CrossRef]
8. Trivedi, C. Investigations of Compressible Turbulent Flow in a High-Head Francis Turbine. *J. Fluids-Eng.-Trans. ASME* **2018**, *140*, 011101. [CrossRef]
9. Bucur, D.M.; Dunca, G.; Calinoiu, C. Experimental vibration level analysis of a Francis turbine. *IOP Conf. Ser. Earth Environ. Sci.* **2012**, *15*, 062056. [CrossRef]
10. Wang, F.J.; Li, X.Q.; Min, Y.A.; Zhu, Y.L. Experimental Investigation of Characteristic Frequency in Unsteady Hydraulic Behaviour of a Large Hydraulic Turbine. *J. Hydrodyn. Ser. B* **2009**, *21*, 12–19. [CrossRef]
11. Favrel, A.; Müller, A.; Landry, C.; Yamamoto, K.; Avellan, F. Study of the vortex-induced pressure excitation source in a Francis turbine draft tube by particle image velocimetry. *Exp. Fluids* **2015**, *56*, 1–15. [CrossRef]
12. Faria, M.T.C.; Paulino, O.G.; Oliveira, F.H.A.; Barbosa, B.H.G.; Martinez, C.B. Influence of Mechanical Draft Tube Fish Barrier on the Hydraulic Thrust of Small Francis Turbines. *J. Hydraul. Eng.* **2010**, *136*, 924–928. [CrossRef]
13. Kazakov, Y.A.; Pelinskii, A.A. Experimental investigation of the axial force in a submersible, electric well pump. *Chem. Pet. Eng.* **1970**, *6*, 262–263. [CrossRef]
14. Tao, R.; Xiao, R.; Liu, W. Investigation of the flow characteristics in a main nuclear power plant pump with eccentric impeller. *Nucl. Eng. Des.* **2018**, *327*, 70–81. [CrossRef]
15. Alligné, S.; Maruzewski, P.; Dinh, T.; Wang, B.; Fedorov, A.; Iosfin, J.; Avellan, F. Prediction of a Francis turbine prototype full load instability from investigations on the reduced scale model. *IOP Conf. Ser. Earth Environ. Sci.* **2010**, *12*, 012025. [CrossRef]
16. Müller, A.; Favrel, A.; Landry, C.; Avellan, F. Fluid–structure interaction mechanisms leading to dangerous power swings in Francis turbines at full load. *J. Fluids Struct.* **2017**, *69*, 56–71. [CrossRef]
17. Magnoli, M.V. Numerical Simulation of Pressure Oscillations in Large Francis Turbines at Partial and Full Load Operating Conditions and Their Effects on the Runner Structural Behaviour and Fatigue Life. Ph.D. Thesis, Technische Universität München, Munich, Germany, 2014.
18. Zhang, R.K.; Cai, Q.D.; Wu, J.Z.; Wu, Y.L.; Liu, S.H.; Zhang, L. The physical origin of severe low-frequency pressure fluctuations in giant Francis turbines. *Mod. Phys. Lett. B* **2005**, *19*, 1527–1530. [CrossRef]
19. Geng, Q. Experimental Research on Pressure Pulsation and Stability of Giant Francis Turbine. *IOP Conf. Ser. Earth Environ. Sci.* **2021**, *676*, 012141. [CrossRef]
20. Li, S. Tiny bubbles challenge giant turbines: Three Gorges puzzle. *Interface Focus* **2015**, *5*, 20150020. [CrossRef]
21. Flores, E.; Bornard, L.; Tomas, L.; Liu, J.; Couston, M. Design of large Francis turbine using optimal methods. *IOP Conf. Ser. Earth Environ. Sci.* **2012**, *15*, 022023. [CrossRef]
22. Tan, Y.; Li, Y.P.; Si, H.S. Start-up and Commissioning Tests on the Stability of a Giant Hydro-turbine Unit. *Hydropower New Energy* **2021**, *35*, 25–27.
23. You, P.; Ji, H.Z.; Tang, W.Q. Analysis of the Vibration of Giant Hydro-turbine Generator Unit. *Hydropower New Energy* **2021**, *35*, 35–38.
24. Gong, R.Z.; Wang, H.G.; Yao, Y.; Shu, L.F.; Huang, Y.J. Numerical simulation of pressure fluctuation in 1000 MW Francis turbine under small opening condition. *IOP Conf. Ser. Earth Environ. Sci.* **2012**, *15*, 062038. [CrossRef]
25. Liu, C.; Hu, B.; Huang, X.; Kang, T.; Zhou, L.; Liu, Z.; Wang, Z. Effects of Head and Discharge on Internal Flow Characteristics of a High-Quality Installed 1 GW Francis Turbine. In Proceedings of the 2022 International Conference on Environmental Science and Green Energy (ICESGE), Shenyang, China, 9–11 December 2022; pp. 222–227.
26. Chen, H.; Lu, Y.; Liu, K.; Zhang, Z.; Li, H.; Huang, X.; Zhao, W.; Wang, Z. Study on the Internal Flow Characteristics of Long and Short Blade Runners of a 1000 MW Francis Turbine under Different Opening Conditions. *Processes* **2023**, *11*, 1796. [CrossRef]
27. Trivedi, C.; Cervantes, M.J.; Gandhi, B.K.; Dahlhaug, O.G. Experimental and Numerical Studies for a High Head Francis Turbine at Several Operating Points. *ASME J. Fluids Eng.* **2013**, *135*, 111102. [CrossRef]

28. Roache, P.J. Quantification of uncertainty in computational fluid dynamics. *Annu. Rev. Fluid Mech.* **1997**, *29*, 123–160. [CrossRef]
29. Kim, H.-H.; Rakibuzzaman, M.; Kim, K.; Suh, S.-H. Flow and Fast Fourier Transform Analyses for TipClearance Effect in an Operating Kaplan Turbine. *Energies* **2019**, *12*, 264. [CrossRef]